applied sciences

MDPI

Article

Structural, Magnetic and Mechanical Properties of Nd_{16} $(Fe_{76-x}Co_x)B_8$ $0 \leq x \leq 25$ Alloys

Juan Sebastián Trujillo Hernández [1,2,3,*], Ahmed Talaat [4], Jesús Tabares [1], Dagoberto Oyola Lozano [3], Humberto Bustos Rodríguez [3], Hugo Martínez Sánchez [2] and German Antonio Pérez Alcázar [1]

1 Facultad de Ciencias Naturales y Matemáticas, Universidad de Ibagué, Ibagué 730007, Colombia; trujillohernandezjuansebastian@gmail.com (J.T.); js_trujillo5@hotmail.com (G.A.P.A.)
2 Departamento de Física, Universidad del Valle, A. A., Cali 25360, Colombia; santiago3146@hotmail.com
3 Departamento de Física, Universidad del Tolima, Ibagué 730006299, Tolima, Colombia; juan.sebastian.trujillo@correounivalle.edu.co (D.O.L.); juan.trujillo.02@estudiantesunibague.edu.co (H.B.R.)
4 Department of Mechanical Engineering & Materials Science, Swanson School of Engineering, University of Pittsburgh, PA 15261, USA; ahmedtalaatfarag@gmail.com
* Correspondence: juan.trujillo@unibague.edu.co

Received: 23 July 2020; Accepted: 6 August 2020; Published: 14 August 2020

Abstract: In this work, the structural, magnetic and mechanical properties of $Nd_{16}Fe_{76-x}Co_xB_8$ alloys with a varying Co content of x = 0, 10, 20 and 25 were experimentally investigated by X-ray diffraction (XRD), Mössbauer spectrometry (MS) and vibrating sample magnetometry (VSM) at room temperature (RT), and microhardness tests were performed. The system presented hard $Nd_2Fe_{14}B$ and the $Nd_{1.1}Fe_4B_4$ phases for samples with x = 0; when the concentration increased to x = 20 and 25, the CoO phase appeared. All MS data showed ferromagnetic behavior (eight sextets: sites 16k1, 16k2, 8j1, 8j2, 4c, 4e, sb) associated with the hard and soft magnetic phases, and one paramagnetic component (doublet: site d) associated with the minority $Nd_{1.1}Fe_4B_4$ phase, which was not identified by XRD. All samples were magnetically hard and presented hard magnetic behavior. The increase of Co content in these samples did not improve the hard magnetic properties but increased the critical temperature of the system and decreased the crystallite size of the hard phase. There was a general tendency towards increased microhardness with cobalt content that was attributable to cobalt doping, which reduces the lattice parameters and porosities within the sample, improving its hardness.

Keywords: Mössbauer spectroscopy; X-ray diffraction; vibrating sample magnetometry; NdFeB magnets

1. Introduction

NdFeB permanent magnets have been investigated since 1983 [1–3] and continue to be investigated [4,5] due to their high energy density (~450 kJm^{-3}) [6], which makes them useful for a number of different applications including acoustic transducers, air conditioning, electric bikes, wind turbines, hybrid and electric cars and hard disk drives, among others [7]. For these reasons, efforts are being devoted to obtaining an improvement in their magnetic and physical properties. Nanocomposite permanent magnets are composed of soft (α-Fe or Fe_3B) and hard ($Nd_2Fe_{14}B$) nanocrystalline magnetic phases and attract a great deal of interest because they exhibit unusual properties, such as a remanence relation (Mr/Ms) larger than 0.5 (the Stoner–Wohlfarth limitation) due to the exchange coupling between these two phases [8]. Among earlier works into nanocomposite magnet, a study was carried out by Coehoorn, R et al. [9] that investigated $Fe_3B/Nd_2Fe_{14}B$ with magnetic properties of 0.3 T and 93 kJm^{-3} for coercive and magnetic energy, respectively. After these works, different theoretical

models [10–12] were proposed in order to improve the general understanding of exchange-coupled nanocomposite magnets. A number of studies were reported for thin films; for example, Cui, W et al. [13] investigated $Nd_2Fe_{14}B$/FeCo anisotropic nanocomposite films and obtained values of the maximum energy product between 400 and 500 kJm^{-3} through an exchange-coupling mechanism. On the other hand, Yang. F et al. [4] recently investigated bonded magnets of NdFeB with $SrFe_{12}O_{19}$ ferrite by additive manufacturing (3D printing); for a sample with 20 wt% of ferrite, they obtained a relatively low surface roughness of ~6 μm and a tensile strength of 12 MPa. However, they obtained a decrease in the magnetic properties of saturation magnetization (M_s), remanent magnetization (M_r), coercive field (H_c) and maximum energy product $(BH)_{max}$ upon increasing the content wt% of ferrite. Other recent work on the NdFeB system using the same principle was reported in [5], where the phase and hyperfine structure of melt-spun nanocrystalline $(Ce_{1-x}Nd_x)_{16}Fe_{78}B_6$ alloys were studied. These results suggest that alloys are composed specifically of the $(NdCe)_2Fe_{14}B$ phase; however, phases such as $(CeNd)Fe_2$ and $(CeNd)Fe_4B_4$ have also been identified. The Mössbauer fit was carried out using six sextets and two doublet components; the average magnetic hyperfine field using Mössbauer and the magnetic properties M_s, H_c and $(BH)_{max}$ increased for compositions from x = 0 to x = 0,7.These properties are sensible to the type of elements of the hard [14–19] and soft phases [14,20], to the grain size of the hard phase [15,16,21–24] and to the different techniques used to prepare them [25–36]. In addition to studies of magnetic properties, it is also important to consider the mechanical properties of permanent magnets. Many efforts have been made to find ways to improve these mechanical properties [2,37]; previous efforts have mainly focused on modifying the compositions by the addition of doping elements such as Al, Ti, Nb, Ga, Cu, Cr, Zr, etc. [38,39].

Considering the tetragonal crystalline stature of Co with uniaxial anisotropy and an atomic ratio of 1.25 Å, comparable to that of Fe (1.26 Å), we studied the effect of the addition of Co on the structural, magnetic and mechanical properties of $Nd_{16}Fe_{76-x}Co_xB_8$ alloys (x = 0, 10, 20, and 25) obtained through an arc-furnace and characterized them by X-ray diffraction (XRD), Mössbauer spectrometry (MS), vibrating sample magnetometry (VSM) and microhardness studies.

2. Materials and Methods

Alloys of the $Nd_{16}Fe_{76-x}Co_xB_8$ (x = 0, 10, 20, and 25) system were prepared by mixing and compacting high-purity fine powders (purity higher than 99.9%) of Fe, Nd, B and Co. These samples were prepared by the arc-melting method under an Ar atmosphere. The resulting ingots were compacted into pellets and encapsulated and evacuated under vacuum, in a quartz ampule, and finally heat treated at 1073 K for 30 min, followed by water quenching. Afterwards, the ingots were partially hand ground (particle size below 100 μm). All prepared samples were characterized by MS, XRD, VSM and microhardness tests. Mössbauer measurements were performed in a constant acceleration spectrometer at room temperature with transmission geometry using a $^{57}Co(Rh)$ source of 25 mCi. All spectra were fitted with the MOSFIT program [40], and the isomeric deviation values were in reference to α-Fe. The XRD measurements were performed at room temperature using Cu-Kα radiation in transmission geometry in the 2θ range between 20° and 90°. The patterns were refined by using the GSAS program [41], which is based on the Rietvelt method combined with Fourier analysis, to describe the broadening of the lines. This refinement yielded the average values of the lattice parameters and of the crystallite sizes and quantified the obtained structural phases. A physical property measurement system (PPMS) equipped with a vibrating sample magnetometer (VSM) was used for magnetic measurements up to 3T. The demagnetization factor of the randomly shaped particles was not taken into consideration. The measurements were made at the Excellence Centre for New Materials (CENM) of Universidad del Valle, Colombia. Vickers hardness tests were performed on heat-treated samples, which were polished to a mirror finish with alumina with a 0.05 μm particle size. Microhardness maps were created with an automated Leco AMH43 microhardness device, on different areas of the samples, applying a load of 200 g and a holding time of 15 s.

3. Results

3.1. XRD

Figure 1 shows the XRD patterns obtained for samples with different Co concentrations. These patterns reveal that all samples presented a tetragonal $Nd_2Fe_{14}B$ hard phase (space group P42/mmm) and an $Nd_{1.1}Fe_4B_4$ phase (tetragonal structure and orthorhombic space group *Pccn*) [42–45]. Additionally, a CoO phase (Wurzita structure and space group *P63mc*) was detected for high concentrations of Co (x = 20 and 25). It can be noted that the intensity of the peaks corresponding to the $Nd_2Fe_{14}B$ phase was slightly reduced and those of $Nd_{1.1}Fe_4B_4$ increased when the Co content increased.

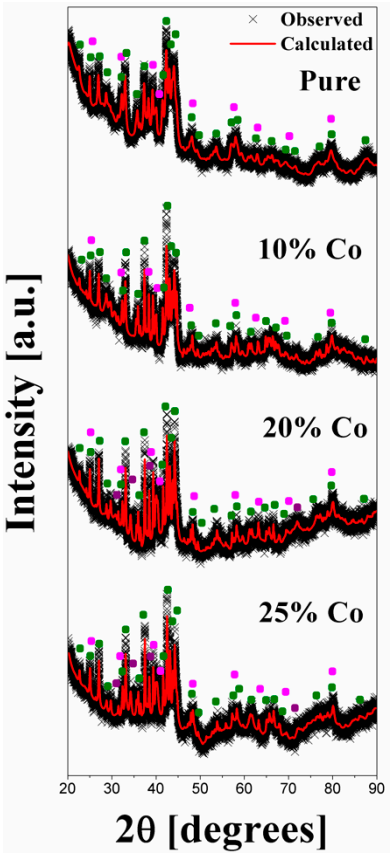

Figure 1. X-ray diffraction (XRD) patterns of the $Nd_{16}Fe_{76-x}Co_xB_8$ samples with x = 0, 10, 20, and 25 at room temperature, when • $Nd_2Fe_{14}B$, • $Nd_{1.1}Fe_4B_4$ and • CoO.

Rietveld refinement allowed us to determine the type of structures with these alloys. The parameter values for samples with a stoichiometry of $Nd_{16}Fe_{76-x}Co_xB_8$ with x = 0, 10, 20 and 25 are reported in Table 1. These data indicate that the crystallite size for $Nd_{1.1}Fe_4B_4$ and $Nd_2Fe_{14}B$ phases was in the nanometer range, from 5 to 90 nm. The crystallite size parallel to the $Nd_{1.1}Fe_4B_4$ and $Nd_2Fe_{14}B$ phases increases with increased concentrations of cobalt. It can be noted that the two phases of parallel crystallite sizes are greater than the perpendicular ones, indicating that the crystallite shape is not spherical but elongated in that direction. The refinement of the mean crystallite size of the hard phase is required in order to obtain higher remanence values [46,47] and to increase the ferromagnetic exchange coupling between the soft and hard grains [10]. The obtained values of the crystallite size indicate that these melted alloys are nanostructured.

Table 1. Structural parameters of the $Nd_{16}Fe_{76-x}Co_xB_8$ samples with x = 0, 10, 20, and 25.

PHASE			$Nd_2Fe_{14}B$			
% Co	**% Phase ± 0.3**	***a*[Å] ± 0.001**	***c*[Å] ± 0.001**	**Vol. [Å^3] ± 0.6**	**Φ ⊥ [nm] ± 1.7**	**Φ [nm] ± 1.7**
0	83.8	8.814	12.210	948.7	19.3	25.0
10	68.8	8.799	12.174	942.7	32.4	48.3
20	60.5	8.768	12.138	933.2	55.0	94.8
25	63.5	8.762	12.136	931.9	44.5	81.0
PHASE			$Nd_{1.1}Fe_4B_4$			
% Co	**% Phase ± 0.3**	***a*[Å] ± 0.001**	***c*[Å] ± 0.001**	**Vol. [Å^3] ± 0.6**	**Φ⊥ [nm] ± 1.0**	**Φ[nm] ± 1.0**
0	15.9	7.113	35.632	1802.9	64.7	5.2
10	31.2	7.096	35.090	1769.9	85.7	10.7
20	33.1	7.108	35.126	1761.1	52.6	3.8
25	28.7	7.100	34.993	1764.6	32.3	15.5
PHASE			*CoO*			
% Co	**% Phase ± 0.4**	***a*[Å] ± 0.001**	***c*[Å] ± 0.001**	**Vol. [Å^3] ± 0.2**	**Φ⊥ [nm] ± 2.0**	**Φ[nm] ± 2.0**
0	–	–		–	–	–
10	–	–		–	–	–
20	6.4	3.185	5.249	46.1	19.0	22.6
25	7.7	3.240	5.234	47.61	38.8	25.3

Table 1 shows the quantitative evolution with the Co content of the weight fraction of the different obtained phases. It can be noted that the Co also decreases the stability of the hard phase, and the decomposition of this phase is conducive to the increase of the $Nd_{1.1}Fe_4B_4$ phase.

Figure 2a,b shows the behavior of the lattice parameters with respect to the cobalt concentration of the $Nd_2Fe_{14}B$ and $Nd_{1.1}Fe_4B_4$ phases for all samples. It is observed that, for x = 0, 10, 20 and 25, the lattice parameters *a* and *c* of $Nd_2Fe_{14}B$ and $Nd_{1.1}Fe_4B_4$ phases decrease considerably with the variation of the concentration of cobalt. This behavior is a consequence of the substitution of Fe by Co atoms, which has an atomic radius (1.25 Å) lower than the atomic radius of Fe (1.26 Å), causing the lattice to reduce. These parameters are consistent with those reported in the literature [48,49].

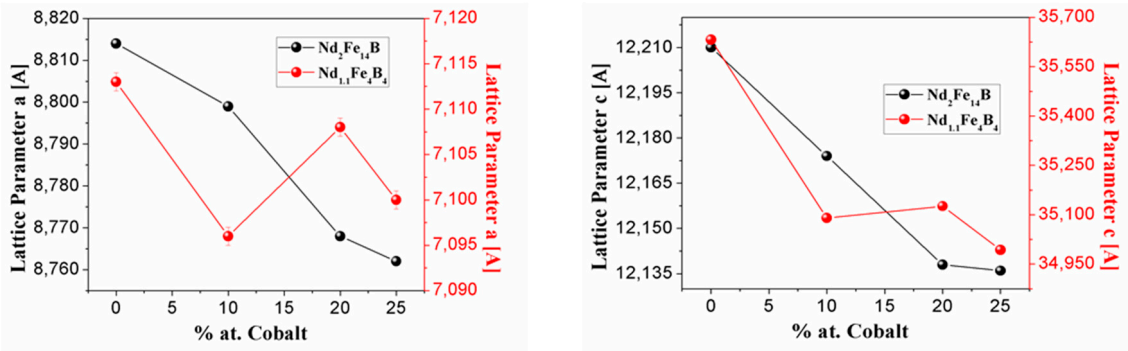

(**a**) (**b**)

Figure 2. (**a**) Lattice parameter *a* as a function of the Co content of the $Nd_2Fe_{14}B$ and $Nd_{1.1}Fe_4B_4$ phases. (**b**) Lattice parameter *c* as a function of the Co content of the $Nd_2Fe_{14}B$ and $Nd_{1.1}Fe_4B_4$ phases.

3.2. Mossbauer Results

The Mössbauer spectra of $Nd_{16}Fe_{76-x}Co_xB_8$ (x = 0, 10, 20 and 25) samples, collected at RT, are shown in Figure 3. To fit these spectra, several subspectra were required, which were associated with the $Nd_2Fe_{14}B$, α-Fe and $Nd_{1.1}Fe_4B_4$ phases. The last phase was not identified by XRD. Seven sextets were used to fit the magnetic part of the spectra, with six of them corresponding to those

reported for the hard phase ($16k_1$, $16k_2$, $8j_1$, $8j_2$, 4c and 4e) and the other corresponding to the α-Fe phase (s^b) reported by Hernandez et al. [50–52]. As can be observed, the Mössbauer spectrum of the sample with x = 0 is typical of the $Nd_2Fe_{14}B$ phase [8]. It was necessary to add a small doublet (site d) in order to obtain the best fit, and this was attributed to the paramagnetic $Nd_{1.1}Fe_4B_4$ phase [50]. The Mössbauer parameters, such as the hyperfine magnetic field (H_{hf}), isomer shift (IS), quadrupole splitting (QS) and area of each subspectra, are listed in Table 2. The value of line width (Γ) takes values of 0.33 mm/s for all sextets and 0.40 mm/s for doublets, which is attributable to the degree of disorder of the samples.

Table 2. Hyperfine parameters: hyperfine field H_{hf}, relative area and sites of the Mössbauer spectra of the $Nd_{16}Fe_{76-x}Co_xB_8$ samples with x = 0, 10, 20 and 25.

% at Co	Phase	Site	[%]Area ± 0.1	H_{hf}[T] ± 0.1
X = 0 **($N_{16}Fe_{76}B_8$)**	**$Nd_{1.1}Fe_4B_4$**	d	8.4	0
	αFe	s^b	4.0	330
	$Nd_2Fe_{14}B$	$16k_1$	14.3	292.4
		$16k_2$	15.7	310.5
		$8j_1$	13.2	274.7
		$8j_2$	11.0	344.9
		4c	23.9	283.7
		4e	9.4	242.3
X = 10 **($N_{16}Fe_{66}Co_{10}B_8$)**	**$Nd_{1.1}Fe_4B_4$**	d	6.4	0
	αFe	s^b	5.0	330
	$Nd_2Fe_{14}B$	$16k_1$	20.9	296.8
		$16k_2$	7.9	327.,1
		$8j_1$	16.7	268.7
		$8j_2$	10.8	350.5
		4c	22.5	296.4
		4e	9.7	242.8
X = 20 **($N_{16}Fe_{56}Co_{20}B_8$)**	**$Nd_{1.1}Fe_4B_4$**	d	6.7	0
	αFe	s^b	3.5	330
	$Nd_2Fe_{14}B$	$16k_1$	16.1	291.1
		$16k_2$	17.6	305.2
		$8j_1$	16.7	264.5
		$8j_2$	11.9	330.6
		4c	16.8	280.1
		4e	10.7	242.5
X = 25 **($N_{16}Fe_{51}Co_{25}B_8$)**	**$Nd_{1.1}Fe_4B_4$**	d	6.9	0
	αFe	s^b	3.1	330
	$Nd_2Fe_{14}B$	$16k_1$	21.3	292.5
		$16k_2$	15.7	294.6
		$8j_1$	14.4	261.8
		$8j_2$	11.4	329.6
		4c	19.0	265.7
		4e	8.3	229.9

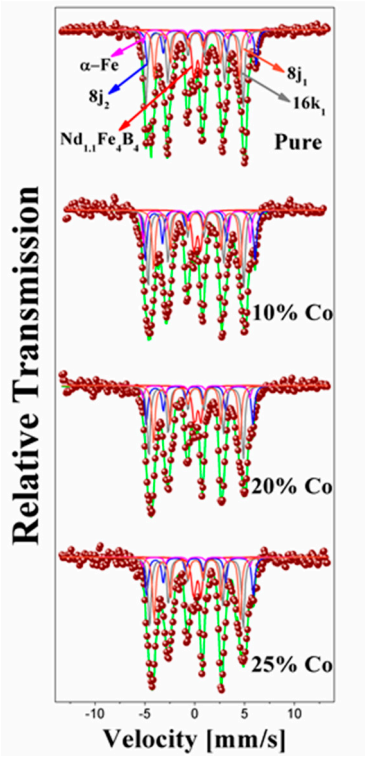

Figure 3. Mössbauer spectra of the $Nd_{16}Fe_{76-x}Co_xB_8$ samples with x = 0, 10, 20 and 25 at room temperature.

Figure 4a shows the variation of the hyperfine field, H_{hf}, of the different inequivalent Fe sites in the $Nd_2Fe_{14}B$ hard magnetic phase as a function of Co content. It can be noted that the hyperfine field of the different sites has a tendency to decrease. This decrease is mainly due to the cobalt having a magnetic moment (1.71 μB/atom) lower than the magnetic moment of iron (2.22 μB/atom), and this result suggests that cobalt atoms enter within the lattice of $Nd_2Fe_{14}B$. However, for site 4c and 16k2 a higher rate of decrease of the hyperfine field with the cobalt concentration occurs; only for the 10% increase of cobalt does this result indicate that the cobalt atoms have a preference for substituting iron atoms at those sites. However, for 10% of cobalt, a higher rate of increase of the hyperfine field can occur because, in these sites, there is a higher presence of Fe neighbors than in the other sites for the different concentrations of doping with cobalt. These results agree with those of Liao et al. [52].

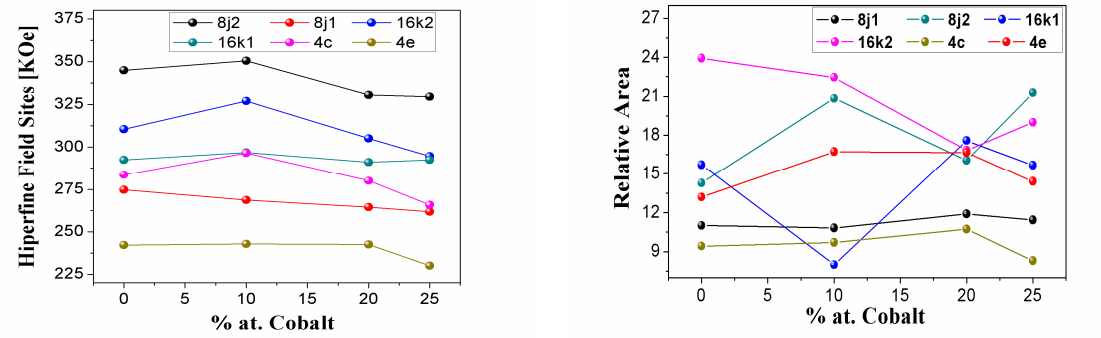

(**a**) (**b**)

Figure 4. (**a**) Hyperfine field of Fe sites (16k1, 16k2, 8j1, 8j2, 4c and 4e) of the hard magnetic phase $Nd_2Fe_{14}B$ as a function of Co content. (**b**) Relative area of Fe sites (16k1, 16k2, 8j1, 8j2, 4c and 4e) of the hard magnetic phase $Nd_2Fe_{14}B$ as a function of Co content.

In Figure 4b, the results are also consistent, which shows a high decrease in the relative area of 4c, confirming the preference of cobalt atoms by replacing iron atoms at these sites, comparing sites 8j1, 8j2, 16k1, 16k2 and 4e, which have a tendency to increase their relative area; thus, the cobalt does not replace iron atoms in these sites, and the ferromagnetism of these sites increases.

It can be observed in Figure 5a that there is a general tendency of the mean hyperfine field (MHF) to decrease as the cobalt content increases. Here, Figure 5a shows a peak at around 10% of doping with cobalt, which corresponds to Figure 4a, where an increase in the sites of hyperfine fields is evidenced due to the high presence of Fe atoms as first neighbors. Figure 5b shows the behavior of the relative area of site d ($Nd_{1.1}Fe_4B_4$) and site s^b (α-Fe) relative to Co content. The diminishing relative area of ˆsite d ($Nd_{1.1}Fe_4B_4$) suggests that substituting iron atoms by cobalt atoms destabilizes the $Nd_{1.1}Fe_4B_4$ phase. Besides, this Figure 5b shows that the relative area of the α-Fe phase decreases with the cobalt content. Only about 10% of cobalt increases the α-Fe phase, which is consistent with the previous results shown in Figures 4a and 5a. These results indicate that cobalt atoms diffuse into the structure of $Nd_2Fe_{14}B$, substituting and expelling iron atoms and producing segregated Fe.

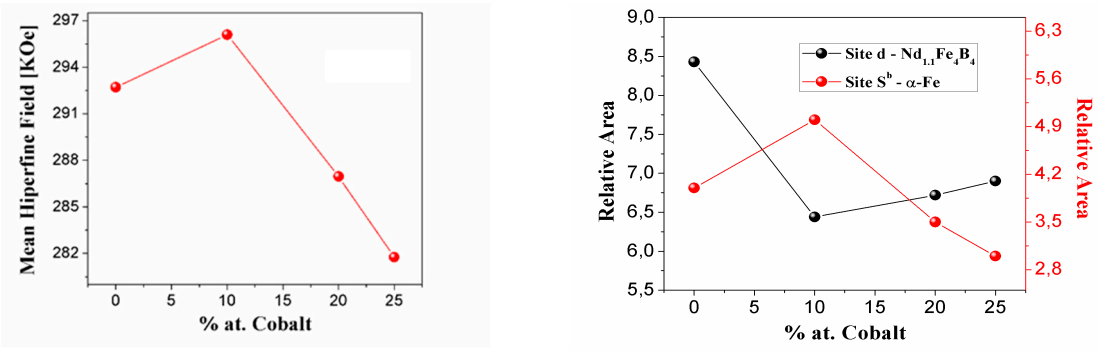

(**a**) (**b**)

Figure 5. (**a**) Mean hyperfine field of the $Nd_{16}Fe_{76-x}Co_xB_8$ samples with x = 0, 10, 20 and 25 at room temperature. (**b**) Variation of relative spectral area of the α-Fe (S^b) and $Nd_{1.1}Fe_4B_4$ (d) sites as a function of Co content.

3.3. Magnetic Properties

Figure 6 shows the hysteresis loops for the alloys with x = 0, 10, 20 and 25. All samples show a predominant $Nd_2Fe_{14}B$ hard magnetic phase. However, the addition of cobalt reduces the size and width of the hysteresis loop, especially for x = 25. These samples reach the saturation magnetization when the fields are higher than 2.5 T. On the other hand, the values of the coercive field H_c decrease with the increase of Co content, as shown in Figure 7a. Despite this decrease in coercivity, all samples still display a hard magnetic character.

Figure 7b shows the behavior of the saturation magnetization M_s and of the remanent magnetization M_r with the concentration of cobalt. It can be concluded that increasing the concentration of cobalt increases the saturation magnetization and decreases the remanent magnetization. This behavior can be explained by the faxt that cobalt has a lower magnetic moment than iron and also stimulates the creation of only one CoO phase, and this does not limit the creation of the $Nd_2Fe_{14}B$ hard magnetic phase. These results agree with those reported by Lin et al. [53]. Further domain structure analysis is needed to shed light on the magnetization process of these exchange-coupled systems upon Co doping.

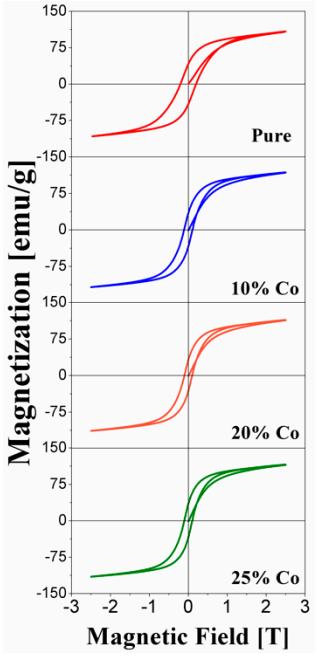

Figure 6. Hysteresis loop of the $Nd_{16}Fe_{76-x}Co_xB_8$ samples with x = 0, 10, 20 and 25 at room temperature.

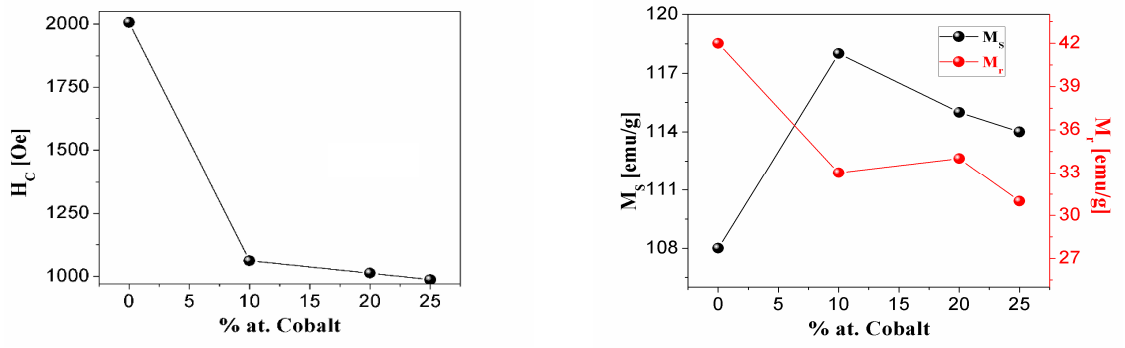

(**a**) (**b**)

Figure 7. (**a**) Variation of coercive field *Hc* as a function of Co content. (**b**) Variation of saturation magnetization M_s and remanent magnetization M_r as a function of Co content.

3.4. Microhardness

The mechanical properties of the studied samples depend mainly on the microstructure, which is determined by the composition, the fabrication process and sintering temperature [17]. We carried out a hardness evolution of the system $Nd_{16}Fe_{76-x}Co_xB_8$ with x = 0, 10, 20 and 25 as a function of the atomic percentage of cobalt. The microhardness values of the samples with respect to the cobalt content are displayed in Figure 8a. A general tendency of microhardness increasing with cobalt content is observed. The heat treatment promotes the diffusion of the cobalt atoms within the NdFeB matrix, increasing the grain size, which in turns reduces the lattice parameter and the porosity in the sample, resulting finally in the improvement of its hardness, as can be seen in the microhardness images presented in Figure 8b.

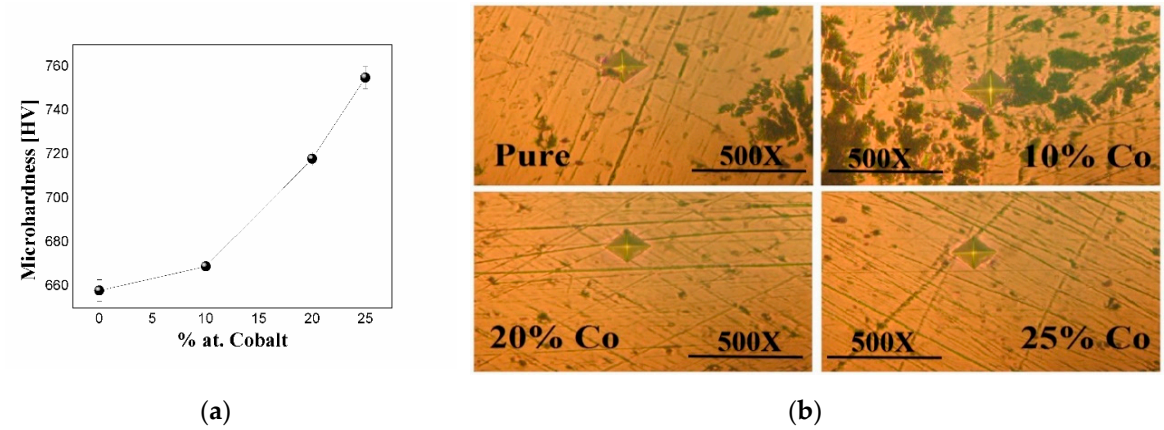

Figure 8. (**a**) Variation of the microhardness as a function of Co content. (**b**) Images of the trace made for obtaining the microhardness at 500× as a function of Co content.

4. Conclusions

From the results of the present work, it can be concluded that the substitution of Fe by Co atoms in the $Nd_{16}Fe_{76-x}Co_xB_8$ nanocomposite alloy decreases the hard magnetic character of the system. The increase of the Co content decreases the stability of the hard phase. The hard phase decreases due the decrease of the 4c site when Co content increases. The magnetic softening of the samples is principally due to the low ferromagnetic coupling between the soft and hard phases. There is a general trend of increasing microhardness with cobalt content, which is attributable to the role of cobalt doping in reducing the lattice parameters and porosities in the sample. In summary, the coupling between NdFeB and Co generates nanostructured systems that favor the formation of hard and soft magnetic phases and improves the ductility conditions, improving the magnetic and mechanical properties of exchange-coupling magnets.

Author Contributions: Conceptualization, J.S.T.H., G.A.P.A., D.O.L.; methodology, J.S.T.H., H.B.R.; software, J.S.T.H., H.M.S.; validation, J.S.T.H., G.A.P.A., D.O.L.; formal analysis, J.S.T.H., A.T.; investigation, J.S.T.H.; writing—original draft preparation, J.S.T.H.; writing—review and editing, A.T.; supervision, D.O.L., J.T.; project administration, D.O.L., G.A.P.A.; funding acquisition, D.O.L., G.A.P.A. All authors have read and agreed to the published version of the manuscript.

Funding: This research was funded by COLCIENCIAS, grant number FP 44842-104-2016 and The Estancia Posdoctoral Colciencias was funded by Convocatoria 811-2018.

Acknowledgments: The authors express special thanks to the Research Office of the Universidad del Tolima and COLCIENCIAS, under Contract FP 80740-415-2019, for the financing of this work. Part of the research was also sponsored by the Army Research Laboratory and was accomplished under Cooperative Agreement Number W911NF-19-2-0030. The views and conclusions contained in this document are those of the authors and should not be interpreted as representing the official policies, either expressed or implied, of the Army Research Laboratory or the U.S. Government. The U.S. Government is authorized to reproduce and distribute reprints for Government purposes notwithstanding any copyright notation herein. The authors would like to thank Anit Giri, from the U.S. Army Research Laboratory for the critical discussion of the results.

Conflicts of Interest: The authors declare no conflict of interest.

References

1. Croat, J.J.; Herbst, J.F.; Lee, R.W.; Pinkerton, F.E. High-energy product Nd-Fe-B permanent magnets. *Appl. Phys. Lett.* **1984**, *44*. [CrossRef]
2. Sagawa, M.; Fujimura, S.; Togawa, N.; Yamamoto, H.; Matsuura, Y. New material for permanent magnets on a base of Nd and Fe (invited). *J. Appl. Phys.* **1984**, *55*. [CrossRef]
3. Hadjipanayis, G.C. Nanophase hard magnets. *J. Magn. Magn. Mater.* **1999**, *200*. [CrossRef]
4. Yang, F.; Zhang, X.; Guo, Z.; Ye, S.; Sui, Y.; Volinsky, A.A. 3D printing of NdFeB bonded magnets with SrFe12O19 addition. *J. Alloy. Compd.* **2019**, *779*. [CrossRef]

5. Zhao, L.Z.; Yu, H.Y.; Guo, W.T.; Zhang, J.S.; Zhang, Z.Y.; Hussain, M.; Liu, Z.W.; Greneche, J.M. Phase and Hyperfine Structures of Melt-spun Nanocrystalline (Ce1-xNdx)16Fe78B6 Alloys. *IEEE Trans. Magn.* **2017**, *53*. [CrossRef]
6. Madugundo, R.; Rama Rao, N.V.; Schönhöbel, A.M.; Salazar, D.; El-Gendy, A.A. Recent Developments in Nanostructured Permanent Magnet Materials and Their Processing Methods. In *Magnetic Nanostructured Materials: From Lab to Fab*; Elsevier: Amsterdam, The Netherlands, 2018.
7. Fischbacher, J.; Kovacs, A.; Gusenbauer, M.; Oezelt, H.; Exl, L.; Bance, S.; Schrefl, T. Micromagnetics of rare-earth efficient permanent magnets. *J. Phys. D Appl. Phys.* **2018**, *51*. [CrossRef]
8. McCallum, R.W.; Kadin, A.M.; Clemente, G.B.; Keem, J.E. High performance isotropic permanent magnet based on Nd-Fe-B. *J. Appl. Phys.* **1987**, *61*. [CrossRef]
9. Coehoorn, R.; de Mooij, D.B.; Duchateau, J.P.W.B.; Buschow, K.H.J. Novel Permanent Magnetic Materials Made by Rapid Quenching. *J. Phys. Colloq.* **1988**, *49*. [CrossRef]
10. Kneller, E.F.; Hawig, R. The exchange-spring magnet: A new material principle for permanent magnets. *IEEE Trans. Magn.* **1991**, *27*. [CrossRef]
11. Fullerton, E.E.; Jiang, J.S.; Bader, S.D. Hard/soft magnetic heterostructures: Model exchange-spring magnets. *J. Magn. Magn. Mater.* **1999**, *200*. [CrossRef]
12. López-Ortega, A.; Estrader, M.; Salazar-Alvarez, G.; Roca, A.G.; Nogués, J. Applications of exchange coupled bi-magnetic hard/soft and soft/hard magnetic core/shell nanoparticles. *Phys. Rep.* **2015**, *553*. [CrossRef]
13. Cui, W.B.; Takahashi, Y.K.; Hono, K. Nd2Fe14B/FeCo anisotropic nanocomposite films with a large maximum energy product. *Adv. Mater.* **2012**, *24*. [CrossRef] [PubMed]
14. Chang, W.C.; Chiou, D.Y.; Wu, S.H.; Ma, B.M.; Bounds, C.O. High performance α-Fe/Nd2Fe14B-type nanocomposites. *Appl. Phys. Lett.* **1998**, *72*. [CrossRef]
15. Kou, X.C.; Dahlgren, M.; Grössinger, R.; Wiesinger, G. Spin-reorientation transition in nano-, micro- and single-crystalline Nd2Fe14B. *J. Appl. Phys.* **1997**, *81*. [CrossRef]
16. Villas-Boas, V.; Romero, S.A.; Missell, F.P. Flash annealing and magnetic interactions in Pr4Fe78B. *J. Appl. Phys.* **1997**, *81*. [CrossRef]
17. Wang, G.P.; Liu, W.Q.; Huang, Y.L.; Ma, S.C.; Zhong, Z.C. Effects of sintering temperature on the mechanical properties of sintered NdFeB permanent magnets prepared by spark plasma sintering. *J. Magn. Magn. Mater.* **2014**, *349*. [CrossRef]
18. Yan, H.Z.; Kong, F.Q.; Xiong, W.; Li, B.Q.; Li, J.; Wang, L. New La-Fe-B ternary system hydrogen storage alloys. *Int. J. Hydrog. Energy* **2010**, *35*. [CrossRef]
19. Hou, B.Y.; Xu, Z.; Peng, S.; Rong, C.; Liu, J.P.; Sun, S. A facile synthesis of SmCo5 magnets from core/shell Co/Sm 2O3 nanoparticles. *Adv. Mater.* **2007**, *19*. [CrossRef]
20. Betancourt, I.; Davies, H.A. Exchange coupled nanocomposite hard magnetic alloys. *Mater. Sci. Technol.* **2010**, *26*. [CrossRef]
21. Oyola Lozano, D.; Zamora, L.E.; Pérez Alcázar, G.A.; Rojas, Y.A.; Bustos, H.; Greneche, J.M. Magnetic and structural properties of the Nd2(Fe 100-xNbx)14B system prepared by arc melting. *Hyperfine Interact.* **2006**, *169*. [CrossRef]
22. You, C.Y.; Takahashi, Y.K.; Hono, K. Fabrication and characterization of highly textured Nd-Fe-B thin film with a nanosized columnar grain structure. *J. Appl. Phys.* **2010**, *108*, 043901. [CrossRef]
23. Cui, B.Z.; Sun, X.K.; Xiong, L.Y.; Cao, S.T.; Zhang, X.X.; Liu, W.; Geng, D.Y.; Zhang, Z.D. Relation between structure and magnetic properties of Nd2(Fe, Co, Mo)14B/α-Fe nanocomposite magnets. *J. Alloy. Compd.* **2002**, *340*. [CrossRef]
24. Valcanover, J.A.; Paduani, C.; Ardisson, J.D.; Pérez, C.A.S.; Yoshida, M.I. Mössbauer effect and magnetization studies of Nd16Fe 76 - XRuxB8 alloys. *Acta Mater.* **2005**, *53*. [CrossRef]
25. Fukagawa, T.; Ohkubo, T.; Hirosawa, S.; Hono, K. Nano-sized disorders in hard magnetic grains and their influence on magnetization reversal at artificial Nd/Nd2Fe14B interfaces. *J. Magn. Magn. Mater.* **2010**, *322*. [CrossRef]
26. Cui, W.B.; Takahashi, Y.K.; Hono, K. Microstructure optimization to achieve high coercivity in anisotropic Nd-Fe-B thin films. *Acta Mater.* **2011**, *59*. [CrossRef]
27. Saito, T. Electrical resistivity and magnetic properties of Nd-Fe-B alloys produced by melt-spinning technique. *J. Alloy. Compd.* **2010**, *505*. [CrossRef]

28. Ma, B.M.; Herchenroeder, J.W.; Smith, B.; Suda, M.; Brown, D.; Chen, Z. Recent development in bonded NdFeB magnets. *J. Magn. Magn. Mater.* **2002**, *239*. [CrossRef]
29. Keavney, D.J.; Fullerton, E.E.; Pearson, J.E.; Bader, S.D. High-coercivity, c-axis oriented Nd2Fe14B films grown by molecular beam epitaxy. *J. Appl. Phys.* **1997**, *81*. [CrossRef]
30. Nishio, T.; Koyama, S.; Kasai, Y.; Panchanathan, V. Low rare-earth Nd–Fe–B bonded magnets with improved irreversible flux loss. *J. Appl. Phys.* **1997**, *81*. [CrossRef]
31. Corfield, M.R.; Williams, A.J.; Harris, I.R. Effects of long term annealing at 1000 °C for 24 h on the microstructure and magnetic properties of Pr-Fe-B/Nd-Fe-B magnets based on Nd16Fe76B8 and Pr16Fe76B. *J. Alloy Compd.* **2000**, *296*. [CrossRef]
32. Yue, M.; Tian, M.; Zhang, J.X.; Zhang, D.T.; Niu, P.L.; Yang, F. Microstructure and magnetic properties of anisotropic Nd-Fe-B magnets produced by spark plasma sintering technique. *Mater. Sci. Eng. B Solid-State Mater. Adv. Technol.* **2006**, *131*. [CrossRef]
33. Pandian, S.; Chandrasekaran, V.; Markandeyulu, G.; Iyer, K.J.L.; Rama Rao, K.V.S. Effect of Al, Cu, Ga, Nb additions on the magnetic properties and microstructural features of sintered NdFeB. *J. Appl. Phys.* **2002**, *92*. [CrossRef]
34. Wang, Z.; Zhou, S.; Zhang, M.; Qiao, Y. High-performance α-Fe/Pr2Fe14B-type nanocomposite magnets produced by hot compaction under high pressure. *J. Appl. Phys.* **2000**, *88*. [CrossRef]
35. Pop, V.; Gutoiu, S.; Dorolti, E.; Isnard, O.; Chicina, I. The influence of short time heat treatment on the structural and magnetic behaviour of Nd 2 Fe 14 B/α-Fe nanocomposite obtained by mechanical milling. *J. Alloy. Compd.* **2011**, *509*. [CrossRef]
36. Neu, V.; Schultz, L. Two-phase high-performance Nd-Fe-B powders prepared by mechanical milling. *J. Appl.' Phys.* **2001**, *90*. [CrossRef]
37. Horton, J.A.; Herchenroeder, J.W.; Wright, J.L.; Easton, D.S. Fracture toughness of Nd2Fei4B magnets. *Mater. Trans. Jim* **1996**, *37*. [CrossRef]
38. Hu, Z.H.; Zhu, M.G.; Li, W.; Lian, F.Z. Effects of Nb on the coercivity and impact toughness of sintered Nd-Fe-B magnets. *J. Magn. Magn. Mater.* **2008**, *320*. [CrossRef]
39. Szymura, S.; Wyslocki, J.J.; Rabinovich, Y.M.; Bala, H. Domain structure, magnetic and mechanical properties of Nd Fe B magnets with different grain size. *Phys. Status Solidi (a)* **1994**, *141*. [CrossRef]
40. Varret, F.; Teillet, J. Unpublished MOSFIT program. Maine University: Le Mans, France.
41. Larson, A.C.; von Dreele, R.B. *General Structure Analysis System (GSAS)*; Los Alamos National Laboratory Report LAUR: Laur, Philippines, 2004.
42. Gao, J.; Volkmann, T.; Roth, S.; Löser, W.; Herlach, D.M. Phase formation in undercooled NdFeB alloy droplets. *J. Magn. Magn. Mater.* **2001**, *234*. [CrossRef]
43. Wang, S.C.; Li, Y. A new structure of Nd1+εFe4B4 phase in NdFeB magnet. *J. Mater. Sci.* **2005**, *40*. [CrossRef]
44. Gang, S.; Lianxi, H.; Erde, W. Preparation, microstructure, and magnetic properties of a nanocrystalline Nd12Fe82B6 alloy by HDDR combined with mechanical milling. *J. Magn. Magn. Mater.* **2006**, *301*. [CrossRef]
45. Sheng, H.; Zeng, X.; Fu, D.; Deng, F. Differences in microstructure and magnetic properties between directly-quenched and optimally-annealed Nd-Fe-B nanocomposite materials. *Phys. B Condens. Matter* **2010**, *405*. [CrossRef]
46. Hadjipanayis, G.C.; Gong, W. Magnetic hysteresis in melt-spun Nd-Fe-Al-B-Si alloys with high remanence. *J. Appl. Phys.* **1988**, *64*. [CrossRef]
47. Manaf, A.; Buckley, R.A.; Davies, H.A. New nanocrystalline high-remanence Nd-Fe-B alloys by rapid solidification. *J. Magn. Magn. Mater.* **1993**, *128*. [CrossRef]
48. Bolzoni, F.; Gavigan, J.P.; Givord, D.; Li, H.S.; Moze, O.; Pareti, L. 3d magnetism in R2Fe14B compounds. *J. Magn. Magn. Mater.* **1987**, *66*. [CrossRef]
49. Sagawa, M.; Hirosawa, S.; Yamamoto, H.; Fujimura, S.; Matsuura, Y. Nd-Fe-B Permanent Magnet Materials. *Jpn. J. Appl. Phys.* **1987**, *26*. [CrossRef]
50. Hernández, J.S.T.; Tabares, J.A.; Alcázar, G.A.P. Structural, magnetic, and mechanical hardness characterization of the alloy Nd16(Fe76−xNix)B8 with x = 0, 10, 20, and 25. *Appl. Phys. A Mater. Sci. Process.*. [CrossRef]
51. Dai, S.; Morrish, A.H.; Zhou, X.Z.; Hu, B.P.; Zhang, S.G. Mössbauer study of the permanent-magnet material Nd 2(Fe1-xNix)14B. *J. Appl. Phys.* **1988**, *63*. [CrossRef]

52. Liao, L.X.; Altounian, Z.; Ryan, D.H. Cobalt site preferences in iron rare-earth-based compounds. *Phys. Rev. B* **1993**, *47*. [CrossRef]
53. Lin, C.; Liu, Z.X.; Sun, Y.X.; Bai, C.X.; Zhao, T.S. Effect of exchange interaction on spin reorientation in the Nd2Fe14B system. *Phys. Rev. B* **1989**, *39*. [CrossRef]